Hot electrons in low-dimensional phonon systems

S.-X. Qu,[1,*] A. N. Cleland,[2] and M. R. Geller[1]
[1]*Department of Physics and Astronomy, University of Georgia, Athens, Georgia 30602-2451, USA*
[2]*Department of Physics, University of California, Santa Barbara, California 93106, USA*
(Received 7 October 2005; revised manuscript received 25 October 2005; published 6 December 2005)

A simple bulk model of electron-phonon coupling in metals has been partially successful in explaining experiments on metal films that actually involve surface- or other low-dimensional phonons. However, by an exact application of this standard model to a semi-infinite substrate with a free surface, making use of the actual vibrational modes of the substrate, we show that such agreement is fortuitous, and that the model actually predicts a low-temperature crossover from the familiar T^5 temperature dependence to a stronger $T^6 \log T$ scaling. Comparison with existing experiments suggests a widespread breakdown of the standard model of electron-phonon coupling in metals.

DOI: 10.1103/PhysRevB.72.224301 PACS number(s): 63.22.+m, 63.20.Kr, 85.85.+j

I. INTRODUCTION

There has been great progress in the efforts to reach the quantum limit of thermal conduction,[1,2] where energy is carried by one-dimensional (1D) channels of coherent phonons, the single-phonon or quantum "optics" regime of phonon dynamics,[3–6] and the quantum limit of nanoelectromechanical systems.[7–12] In addition to their interest for investigating fundamental phonon physics and macroscopic quantum phenomena, low-dimensional phonon systems might enable sensors, such as nanoscale bolometers and calorimeters,[3,13,14] with unprecedented sensitivity, and may also find applications in quantum information processing.[6,7,15,16] In contrast to low-dimensional electron systems, which are typically produced in semiconductor nanostructures by a combination of band gap engineering and electrostatic confinement, low-dimensional phonon systems require mechanical isolation from their environments and are realized in freely suspended structures. The phonon distributions in these systems are controlled *in situ* by thermal coupling with metallic thin-film heaters, and are measured via thermometry on the conduction electrons. But what is the relation between the electron and phonon temperatures? Electrons and phonons are known to become thermally isolated at low temperatures, leading to pronounced "hot electron" effects,[17,18] where the electron and phonon temperatures differ considerably. Understanding low-dimensional phonon systems therefore depends crucially on understanding the thermal coupling between the electron and phonon subsystems.

A widely used standard model of low temperature electron-phonon thermal coupling in bulk metals[17–19] assumes (i) a clean three-dimensional (3D) free-electron gas with a spherical Fermi surface, rapidly equilibrated to a temperature T_{el}; (ii) a continuum description of the acoustic phonons, which have a temperature T_{ph}; (iii) a negligible Kapitza-like thermal boundary resistance[20] between the metal and any surrounding dielectric, an assumption that is usually justified experimentally; and (iv), a deformation-potential electron-phonon interaction, expected to be dominant at long-wavelengths. In a bulk metal, the net rate P of thermal energy transfer between the electron and phonon subsystems is[18]

$$P = \Sigma V_{el}(T_{el}^5 - T_{ph}^5), \tag{1}$$

where V_{el} is the volume of the metal, and

$$\Sigma \equiv \frac{8\zeta(5)k_B^5\epsilon_F^2 N_{el}(\epsilon_F)}{3\pi\hbar^4\rho v_F v_l^4}. \tag{2}$$

Here ζ is the Riemann zeta function, ϵ_F is the Fermi energy, N_{el} is the electronic density of states (DOS) per unit volume, ρ is the mass density, v_l is the bulk longitudinal sound speed, and v_F is the Fermi velocity. For a given power P applied to the film, we can solve (1) for the relation between T_{el} and T_{ph}.

This model, which has no adjustable parameters, has successfully explained some experiments,[2,18,19] but others report a power-law temperature dependence with significantly smaller exponents,[21,22] indicating an enhanced electron-phonon coupling at low temperatures. However, the experiments typically involve heating measurements in thin metal films deposited on semiconducting or insulating substrates, and the relevant phonons at low temperature are strongly modified by the exposed stress-free surface. There has always been the question of how the surface would modify the bulk result (1). An experimental attempt to directly probe such phonon-dimensionality effects was carried out by DiTusa *et al.*,[22] who intentionally suspended some of their samples, necessarily modifying the vibrational spectrum, although they found no significant difference from their supported films. In this paper, we argue that the paradox reported in Ref. 22 is widespread, and all experiments known to us on supported films actually contradict the standard model when that model is modified to account for the actual vibrational modes present in a realistic supported-film geometry, illustrated in Fig. 1. Our results have important implications for the interpretation of experiments on a wide variety of low-dimensional phonon systems, and suggest that future efforts on the electron-phonon coupling problem, rather than focusing on reduced-dimensionality effects, should be redirected towards understanding a breakdown of the standard metallic electron-phonon interaction model itself.

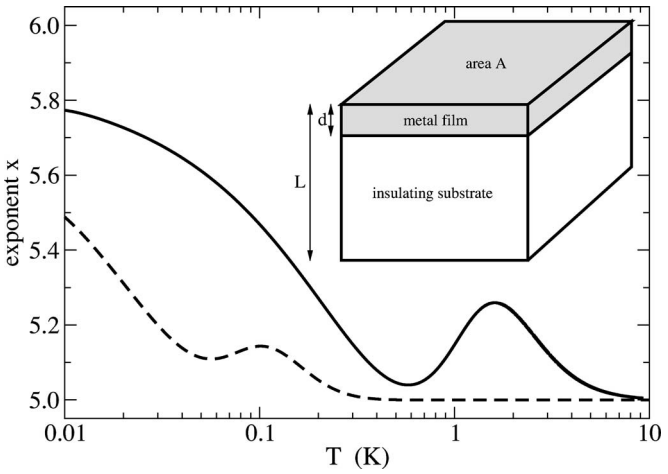

FIG. 1. (Inset) Conducting film of thickness d attached to insulator. The top surface of the metal is stress free. (Main) Temperature dependence of the thermal power exponent x for a 10 nm (solid curve) and 100 nm (dashed curve) Cu film.

II. GENERAL EXPRESSION FOR THE RATE OF THERMAL ENERGY TRANSFER

The Hamiltonian we consider (suppressing spin) is

$$H = \sum_{\mathbf{k}} \epsilon_{\mathbf{k}} c_{\mathbf{k}}^{\dagger} c_{\mathbf{k}} + \sum_{n} \hbar \omega_n a_n^{\dagger} a_n + \delta H, \tag{3}$$

where $c_{\mathbf{k}}^{\dagger}$ and $c_{\mathbf{k}}$ are electron creation and annihilation operators, with $\mathbf{k}$ the momentum, and $a_n^{\dagger}$ and a_n are bosonic phonon creation and annihilation operators. The vibrational modes, labeled by an index n, are eigenfunctions of the continuum elasticity equation

$$v_t^2 \nabla \times \nabla \times \mathbf{u} - v_l^2 \nabla (\nabla \cdot \mathbf{u}) = \omega^2 \mathbf{u} \tag{4}$$

for linear isotropic media, along with accompanying boundary conditions. v_t and v_l are the bulk transverse and longitudinal sound velocities. $\delta H \equiv \frac{2}{3}\epsilon_F \int_{V_{el}} d^3 r \psi^{\dagger} \psi \nabla \cdot \mathbf{u}$ is the deformation-potential electron-phonon interaction, with

$$\mathbf{u}(\mathbf{r}) = \sum_{n} (2\rho\omega_n)^{-1/2} [\mathbf{f}_n(\mathbf{r}) a_n + \mathbf{f}_n^*(\mathbf{r}) a_n^{\dagger}] \tag{5}$$

the quantized displacement field. The vibrational eigenfunctions $\mathbf{f}_n(\mathbf{r})$ are defined to be solutions of the elasticity field equations, normalized over the phonon volume V_{ph} according to $\int_{V_{ph}} d^3 r \mathbf{f}_n^* \cdot \mathbf{f}_{n'} = \delta_{nn'}$. It will be convenient to rewrite the electron-phonon interaction as

$$\delta H = \sum_{\mathbf{k}\mathbf{q}n} [g_{n\mathbf{q}} c_{\mathbf{k}+\mathbf{q}}^{\dagger} c_{\mathbf{k}} a_n + g_{n\mathbf{q}}^* c_{\mathbf{k}-\mathbf{q}}^{\dagger} c_{\mathbf{k}} a_n^{\dagger}], \tag{6}$$

with coupling constant

$$g_{n\mathbf{q}} \equiv \frac{2}{3}\epsilon_F (2\rho\omega_n)^{-1/2} V_{el}^{-1} \int_{V_{el}} d^3 r \nabla \cdot \mathbf{f}_n e^{-i\mathbf{q}\cdot\mathbf{r}}. \tag{7}$$

Note that we allow for different electron and phonon volumes. Our results also apply to wire geometries if the electrons are three dimensional.

The quantity we calculate is the thermal energy per unit time transferred from the electrons to the phonons

$$P \equiv 2 \sum_{\mathbf{k}\mathbf{q}n} \hbar \omega_n [\Gamma_n^{em}(\mathbf{k} \to \mathbf{k}-\mathbf{q}) - \Gamma_n^{ab}(\mathbf{k} \to \mathbf{k}+\mathbf{q})], \tag{8}$$

where

$$\Gamma_n^{em}(\mathbf{k} \to \mathbf{k}-\mathbf{q}) = 2\pi |g_{n\mathbf{q}}|^2 [n_B(\omega_n)+1] n_F(\epsilon_{\mathbf{k}}) [1 - n_F(\epsilon_{\mathbf{k}-\mathbf{q}})] \times \delta(\epsilon_{\mathbf{k}-\mathbf{q}} - \epsilon_{\mathbf{k}} + \omega_n) \tag{9}$$

is the golden-rule rate for an electron of momentum $\mathbf{k}$ to scatter to $\mathbf{k}-\mathbf{q}$ while emitting a phonon n, and

$$\Gamma_n^{ab}(\mathbf{k} \to \mathbf{k}+\mathbf{q}) = 2\pi |g_{n\mathbf{q}}|^2 n_B(\omega_n) n_F(\epsilon_{\mathbf{k}}) [1 - n_F(\epsilon_{\mathbf{k}+\mathbf{q}})] \delta(\epsilon_{\mathbf{k}+\mathbf{q}} - \epsilon_{\mathbf{k}} - \omega_n) \tag{10}$$

is the corresponding phonon absorption rate. n_B is the Bose distribution function with temperature T_{ph} and n_F is the Fermi distribution with temperature T_{el}. The factor of 2 in (8) accounts for spin degeneracy. It is possible to obtain an exact expression for P; the result (suppressing factors of $\hbar$ and k_B) is

$$P = \frac{m^2 V_{el}^2}{8\pi^4} \sum_n \int_0^{\infty} d\omega \delta(\omega - \omega_n) \left(\frac{\omega}{e^{\omega/T_{el}} - 1} - \frac{\omega}{e^{\omega/T_{ph}} - 1} \right) \times \int d^3 k \frac{|g_{n\mathbf{k}}|^2}{|\mathbf{k}|} \times \left[\omega + T_{el} \ln \left(\frac{1 + \exp\left[\left(\frac{m\omega^2}{2k^2} + \frac{k^2}{8m} - \frac{\omega}{2} - \mu \right) \Big/ T_{el} \right]}{1 + \exp\left[\left(\frac{m\omega^2}{2k^2} + \frac{k^2}{8m} + \frac{\omega}{2} - \mu \right) \Big/ T_{el} \right]} \right) \right].$$

The logarithmic term in P can be shown to be exponentially suppressed and negligible in the temperature regime (below 10 K) of interest and will be dropped. Carrying out the $\mathbf{k}$ integration then leads to

$$P = \frac{v_l^4 \Sigma V_{el}}{24\zeta(5)} \int_0^{\omega_D} d\omega F(\omega) \left(\frac{\omega}{e^{\omega/T_{el}} - 1} - \frac{\omega}{e^{\omega/T_{ph}} - 1} \right), \tag{11}$$

where

$$F(\omega) \equiv \sum_n U_n \delta(\omega - \omega_n) \tag{12}$$

is a strain-weighted vibrational DOS, with

$$U_n \equiv \frac{1}{V_{el}} \int_{V_{el}} d^3 r d^3 r' \frac{\nabla \cdot \mathbf{f}_n(\mathbf{r}) \nabla' \cdot \mathbf{f}_n^*(\mathbf{r}')}{|\mathbf{r} - \mathbf{r}'|^2 + a^2}. \tag{13}$$

Here ω_D is the Debye frequency. U_n can be interpreted as an energy associated with mass-density fluctuations interacting via an inverse-square potential,[23] cut off at distances of the order of the lattice constant a. We have reduced the calculation of P to the calculation of $F(\omega)$. Allen[24] has derived a related weighted-DOS formalism.

III. HOT ELECTRON IN LOW DIMENSIONS

We now calculate $F(\omega)$ and P for a metal film of thickness d attached to the free surface of an isotropic elastic continuum with $L\to\infty$; see the inset to Fig. 1. The film and substrate are assumed to have the same elastic parameters, characterized by a mass density ρ and bulk sound velocities v_t and v_l. Where material parameters are necessary we shall assume a Cu film; however, the qualitative behavior we obtain is generic. The evaluation of $F(\omega)$ requires the vibrational eigenfunctions for a semi-infinite substrate with a free surface, which have been obtained in the classic paper by Ezawa.[25] The modes are labeled by a branch index m, taking the five values SH, +, −, 0, and R, by a two-dimensional (2D) wave vector $\mathbf{K}$ in the plane defined by the surface, and by a parameter c with the dimensions of velocity that is continuous for all branches except the Rayleigh branch $m=\mathrm{R}$. With the normalization convention of Ref. 25 we have

$$F(\omega)=\sum_{\mathbf{K}} U_{\mathrm{R}\mathbf{K}}\delta(\omega-c_{\mathrm{R}}K)+\sum_{m\neq\mathrm{R}}\sum_{\mathbf{K}}\int dc\,U_{m\mathbf{K}c}\delta(\omega-cK). \tag{14}$$

The range of parameter c depends on the branch m, as indicated below, and the frequency of mode $m\mathbf{K}c$ is cK.

Turning to an evaluation of (14), the SH branch is purely transverse, so $U_{\mathrm{SH}}=0$. The normalized eigenmodes for the ± branches are[25]

$$\mathbf{f}_{\pm}=\sqrt{\frac{K}{4\pi cA}}\{[\mp\alpha^{-1/2}(e^{-i\alpha Kz}-\zeta_{\pm}e^{i\alpha Kz})+i\beta^{1/2}\times(e^{-i\beta Kz}+\zeta_{\pm}e^{i\beta Kz})]\mathbf{e}_{\mathrm{K}}+[\pm\alpha^{1/2}(e^{-i\alpha Kz}+\zeta_{\pm}e^{i\alpha Kz})+i\beta^{-1/2}(e^{-i\beta Kz}-\zeta_{\pm}e^{i\beta Kz})]\mathbf{e}_z\}e^{i\mathbf{K}\cdot\mathbf{r}},$$

where $\alpha\equiv\sqrt{(c/v_l)^2-1}$ and $\beta\equiv\sqrt{(c/v_t)^2-1}$. Here

$$\zeta_{\pm}\equiv\frac{[(\beta^2-1)\pm 2i\sqrt{\alpha\beta}]^2}{(\beta^2-1)^2+4\alpha\beta},\quad\text{with } |\zeta_{\pm}|=1. \tag{15}$$

Then

$$U_{\pm}=(c^3K/\alpha v_l^4V_{\mathrm{el}})I_{\pm}(Kd,c), \tag{16}$$

where

$$I_{\pm}(Z,c)\equiv\mathrm{Re}\int_0^Z dxdx'\mathsf{K}_0[\sqrt{(x-x')^2+a^2Z^2/d^2}]\times(e^{i\alpha(x-x')}-\zeta_{\pm}e^{i\alpha(x+x')}). \tag{17}$$

K_0 is a modified Bessel function. To obtain $U_{\pm}$ we use translational invariance in the xy plane to write (13) as

$$U_{m\mathbf{K}c}=\frac{A}{V_{\mathrm{el}}}\int_0^d dzdz'\int_A d^2R\frac{\boldsymbol{\nabla}\cdot\mathbf{f}_{m\mathbf{K}c}(\mathbf{R},z)\boldsymbol{\nabla}'\cdot\mathbf{f}^*_{m\mathbf{K}c}(0,z')}{R^2+(z-z')^2+a^2}, \tag{18}$$

where $\mathbf{R}\equiv(x,y)$ is a 2D coordinate vector. Then we scale out K, do the angular integration, and use the identity $\int_0^\infty dRR\mathsf{J}_0(R)[R^2+s^2]^{-1}=\mathsf{K}_0(|s|)$, where J_0 is a Bessel function of the first kind.

Next we consider the $m=0$ branch, for which[25]

$$\mathbf{f}_0=\sqrt{\frac{K}{2\pi\beta cA}}\{[i\mathcal{C}e^{-\gamma Kz}+i\beta e^{-i\beta Kz}+i\beta\mathcal{A}e^{i\beta Kz}]\mathbf{e}_{\mathrm{K}}+[-\gamma\mathcal{C}e^{-\gamma Kz}+ie^{-i\beta Kz}-i\mathcal{A}e^{i\beta Kz}]\mathbf{e}_z\}e^{i\mathbf{K}\cdot\mathbf{r}},$$

where $\gamma\equiv\sqrt{1-(c/v_l)^2}$,

$$\mathcal{A}\equiv\frac{(\beta^2-1)^2-4i\beta\gamma}{(\beta^2-1)^2+4i\beta\gamma},\quad\text{and }\mathcal{C}\equiv\frac{4\beta(\beta^2-1)}{(\beta^2-1)^2+4i\beta\gamma}.$$

Then

$$U_0=(|\mathcal{C}|^2c^3K/\beta v_l^4V_{\mathrm{el}})I_0(Kd,c), \tag{19}$$

where

$$I_0(Z,c)\equiv\int_0^Z dxdx'\mathsf{K}_0[\sqrt{(x-x')^2+a^2Z^2/d^2}]e^{-\gamma(x+x')}. \tag{20}$$

Finally, for the Rayleigh branch

$$\mathbf{f}_{\mathrm{R}}=\sqrt{\frac{K}{\mathcal{K}A}}\left\{\left[ie^{-\varphi Kz}-i\left(\frac{2\varphi\eta}{1+\eta^2}\right)e^{-\eta Kz}\right]\mathbf{e}_{\mathrm{K}}-\left[\varphi e^{-\varphi Kz}-\left(\frac{2\varphi}{1+\eta^2}\right)e^{-\eta Kz}\right]\mathbf{e}_z\right\}e^{i\mathbf{K}\cdot\mathbf{r}}, \tag{21}$$

where $\varphi\equiv\sqrt{1-(c_{\mathrm{R}}/v_l)^2}$, $\eta\equiv\sqrt{1-(c_{\mathrm{R}}/v_t)^2}$, and $\mathcal{K}\equiv(\varphi-\eta)(\varphi-\eta+2\varphi\eta^2)/2\varphi\eta^2$. c_{R} is the velocity of the Rayleigh surface waves, given by $c_{\mathrm{R}}=\xi v_t$, where ξ is the zero between 0 and 1 of $\xi^6-8\xi^4+8(3-2\nu^2)\xi^2-16(1-\nu^2)$, with $\nu\equiv v_t/v_l$. For Cu, $\nu=0.52$ and $\xi=0.93$; hence, $c_{\mathrm{R}}=2.4\times10^5$ cm s^{-1}. Using (21),

$$U_{\mathrm{R}}=(2\pi c_{\mathrm{R}}^4K/\mathcal{K}v_l^4V_{\mathrm{el}})I_{\mathrm{R}}(Kd), \tag{22}$$

where

$$I_{\mathrm{R}}(Z)\equiv\int_0^Z dxdx'\mathsf{K}_0[\sqrt{(x-x')^2+a^2Z^2/d^2}]e^{-\varphi(x+x')}. \tag{23}$$

Carrying out the final summations over $\mathbf{K}$ leads to

$$F(\omega)=\frac{\omega^2}{v_l^4d}\left\{\frac{c_{\mathrm{R}}}{\mathcal{K}}I_{\mathrm{R}}\left(\frac{\omega d}{c_{\mathrm{R}}}\right)+\int_{v_t}^{v_l}dc\frac{|\mathcal{C}|^2}{2\pi\beta}I_0\left(\frac{\omega d}{c},c\right)+\int_{v_l}^{\infty}dc\frac{1}{2\pi\alpha}\left[I_+\left(\frac{\omega d}{c},c\right)+I_-\left(\frac{\omega d}{c},c\right)\right]\right\}. \tag{24}$$

This expression, combined with (11), is our principal result. Evaluation of (24) can be further simplified by the use of the powerful identities

$$I_{\pm}(Z,c)=\mathrm{Re}\left[\left(2Z-\frac{i\zeta_{\pm}}{\alpha}\right)f(Z,\alpha)+\frac{i\zeta_{\pm}}{\alpha}e^{2i\alpha Z}f^*(Z,\alpha)+2i\left(\frac{\partial f(Z,s)}{\partial s}\right)_{s=\alpha}\right], \tag{25}$$

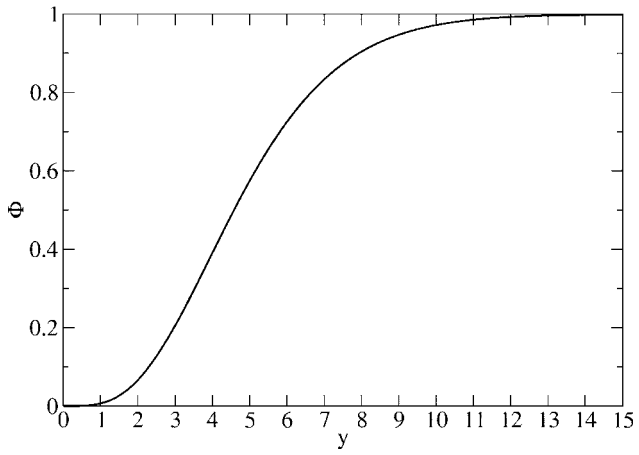

FIG. 2. $\Phi(y)$ function.

$$I_0(Z,c) = \frac{1}{\gamma} f(Z, i\gamma) - \frac{e^{-2\gamma Z}}{\gamma} f(Z, -i\gamma), \tag{26}$$

$$I_R(Z,c) = \frac{1}{\varphi} f(Z, i\varphi) - \frac{e^{-2\varphi Z}}{\varphi} f(Z, -i\varphi), \tag{27}$$

where

$$f(Z,s) \equiv \int_0^Z dx K_0(\sqrt{x^2 + a^2 Z^2/d^2}) e^{isx}, \tag{28}$$

thereby reducing the I_m to a single one-dimensional integral, f.

The I_m have distinct large- and small-Z character, crossing over near $Z=1$. Because of the integration over c in (24), F and P accordingly exhibit a broad crossover behavior. However, once $\omega d < c_R$, all branches will have assumed their low-frequency forms. We define a crossover temperature

$$T^\star \equiv \frac{\hbar c_R}{k_B d} \tag{29}$$

dividing regimes determined by the small and large $\omega d/c_R$ behavior of F. In the large $\omega d/c_R$ limit the $m = \pm$ modes in (24) can be shown to be dominant, and

$$\lim_{\omega d \to \infty} \int_{v_l}^{\infty} dc \frac{1}{\alpha} I_\pm\left(\frac{\omega d}{c}, c\right) = \pi \omega d. \tag{30}$$

Therefore, we obtain

$$F(\omega) \to F_{\text{bulk}}(\omega) \equiv \omega^3 / v_l^4, \tag{31}$$

independent of d, leading to a high-temperature behavior

$$P \to \Sigma V_{\text{el}} [\Phi(\omega_D/T_{\text{el}}) T_{\text{el}}^5 - \Phi(\omega_D/T_{\text{ph}}) T_{\text{ph}}^5], \tag{32}$$

where Σ is the coefficient (2), and where $\Phi(y) \equiv [4!\zeta(5)]^{-1} \int_0^y dx x^4/(e^x - 1)$. $\Phi(10)$ is about 0.97, and $\Phi(y)$ rapidly approaches 1 beyond that, as shown in Fig. 2. Thus, at temperatures above $T^\star$ but sufficiently smaller than the Debye temperature, the Φ factors are equal to unity, and we recover the bulk result (1).

We turn now to the low-temperature asymptotic analysis. Briefly, using the small Z expansion

$$f(Z,s) \to -Z \ln Z + [1 + \ln 2 + \psi(1)] Z - \frac{is}{2} Z^2 \ln Z + \frac{is}{2}\left[\frac{1}{2} + \ln 2 + \psi(1)\right] Z^2 + O(Z^3 \ln Z), \tag{33}$$

where ψ is the Euler polygamma function, we find

$$F(\omega) \to F_{\text{bulk}}(\omega)\left[-\lambda\left(\frac{\omega d}{c_R}\right)\ln\left(\frac{\omega d}{c_R}\right) + O\left(\frac{\omega d}{c_R}\right)\right] \tag{34}$$

in the small $\omega d/c_R$ limit. Here

$$\lambda \equiv \frac{1}{\mathcal{K}} + \int_{v_t}^{v_l} dc \frac{c_R |\mathcal{C}|^2}{2\pi c^2 \beta} + \int_{v_l}^{\infty} dc \frac{c_R [2 - \text{Re}(\xi_+ + \xi_-)]}{2\pi c^2 \alpha} \tag{35}$$

is a constant determined by v_l, v_t, and c_R. Each T^5 function in (1) therefore crosses over at low temperature as

$$T^5 \to -\Lambda\left(\frac{T^6}{T^\star}\right)\ln\left(\frac{T}{T^\star}\right), \tag{36}$$

with $\Lambda = \lambda \pi^6/189\zeta(5)$. For a Cu film, $\lambda \approx 0.815$ and $\Lambda \approx 3.998$. There are also mixed regimes possible, where only one of the two terms in (1) has crossed over.

The most striking consequence of the crossover is that the temperature exponent *increases*. In Fig. 1 we fit P (with either T_{el} or T_{ph} zero) to a power-law T^x with a temperature dependent exponent x, and plot the exponent for a 10 nm ($T^\star = 1.84$ K) and 100 nm ($T^\star = 184$ mK) Cu film. $x(T)$ is nonmonatonic, displaying a pronounced maximum near $T^\star$, and drifts upward as $T \to 0$. Such behavior has not been observed, even though many experiments[2,18,19,22] have achieved $T \ll T^\star$. The physical origin of the crossover is that, at low temperature, the stress-free condition at the metal surface penetrates into the film, reducing the strain and hence electron-phonon coupling there. The characteristic distance over which the boundary condition has an effect is of the order of a bulk wavelength. When $T \gg T^\star$, only a thin outer surface layer of the film has a significantly diminished strain, and bulk behavior is expected. However, when $T \ll T^\star$ the entire metal film experiences a reduced strain.

IV. PREFACTOR

The experiments of Refs. 2 and 19, both using Cu films, observe an approximate T^5 dependence even well below $T^\star$. It is therefore interesting to compare the observed *prefactors* with the coefficient Σ, evaluated for Cu. Using a free-electron gas approximation[26] and measured elastic properties,[27] we obtain 5.97×10^7 W m^{-3} K^{-5}, which is at least an order of magnitude smaller than observed, consistent with our assertion that there is some unidentified mechanism *enhancing* the thermal coupling.

Noble metals are far from free-electron systems because of their complex Fermi surfaces. Here we attempt to address this shortcoming by regarding the Fermi surface quantities

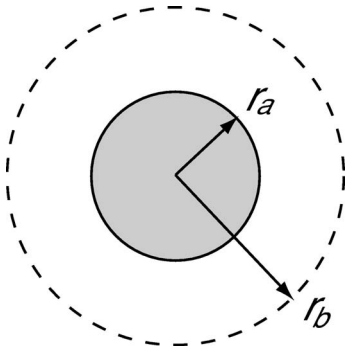

FIG. 3. One of the eight circular patches centered on the ⟨111⟩ and equivalent directions of the Cu Fermi surface. The shaded region represents a section of a cylindrical neck of radius r_a that crosses a hexagonal Brillouin zone boundary. In our Fermi surface model, the Fermi energy changes linearly from $v_a=0.40$ to $v_b=0.75$ times the free-electron value in the annular region $r_a<r<r_b$, and remains 0.75 beyond r_b.

$N_{\rm el}(\epsilon_{\rm F})$ and $v_{\rm F}$ as independently adjustable parameters, to be obtained empirically from heat capacity and cyclotron resonance data. First, the DOS inferred from heat capacity measurements is a factor of 1.38 larger than the free-electron value.[28] Second, the Fermi surface, although largely spherical, extends beyond the first Brillouin zone boundary in the ⟨111⟩ direction, thereby forming cylindrical necks that cross the eight hexagonal zone faces, and cyclotron resonance studies indicate that the Fermi velocity is highly anisotropic near these necks. Therefore, we propose to replace the free-electron value of $v_{\rm F}$ in Eq. (2) with the Fermi-surface average $\bar{v}_{\rm F}$ of the anisotropic velocity field introduced by Lee[29] and by Lengeler *et al.*[30] in their attempts to accurately model cyclotron resonance and heat capacity data.

From Refs. 29 and 30 we deduce that over most of the Fermi surface, $v_{\rm F}$ is approximately 75% of its free-electron value, except within circular patches centered about the ⟨111⟩ and equivalent directions, where it decreases linearly to approximately 40% at the boundaries of the cylindrical necks. We model the Fermi surface as follows: Away from the necks we take the surface to be that of a unit sphere. The radius of the necks, indicated in Fig. 3, are observed to be about 10 deg, or $r_a=0.175$ in our units. The total area of the Fermi surface is $4\pi-8\pi r_a^2$ because of the necks. The average velocity within each annular region of the type shown in Fig. 3, with r_b taken to be twice r_a, is

$$\frac{\int d^2 r v_{\rm F}}{\pi(r_b^2-r_a^2)}=\frac{4v_a+5v_b}{9}=0.59, \tag{37}$$

in units of the free-electron velocity. The relative velocity on the rest of the surface is 75%. Putting everything together we then obtain, for the surface-averaged $v_{\rm F}$,

$$\bar{v}_{\rm F}=0.72\times \text{the free Fermi velocity}. \tag{38}$$

Including these DOS and Fermi velocity corrections in Eq. (2) leads to the modified prefactor

$$\Sigma=1.14\times 10^8 \text{W m}^{-3}\,\text{K}^{-5}, \tag{39}$$

which is still considerably smaller than that measured. We conclude that the experiments of Refs. 2 and 19 do not observe the constant prefactor (2) predicted for Cu.

V. DISCUSSION

Although not included in the model considered here, disorder in a metal film is expected to produce a low-temperature crossover from the T^5 dependence to a T^6 scaling[31] when the thermal wavelength becomes larger than the electron elastic mean free path ℓ, a behavior which has not been observed until very recently.[32] Thus, in the typical "clean" situation where $\ell>d$, the crossover predicted here will be unaffected by disorder, and there will be a window of temperature below $T^\star$ where our results apply, until an even lower temperature where a second crossover to the disordered regime occurs. Furthermore, although thin films are known to also scatter phonons strongly, measured values of the phonon elastic mean free path[33] are still much larger than d in the temperature regime (below 10 K) of interest here.

In conclusion, we argue that a wide variety of experiments contradict the predictions of an essentially exact application of the standard model of electron-phonon thermal coupling in metals to a supported-film geometry, suggesting a widespread breakdown of that model.

ACKNOWLEDGMENTS

A.N.C. was supported by the NASA Office of Space Science under Grant No. NAG5-8669 and by the Army Research Office under DAAD-19-99-1-0226. M.R.G. was supported by the NSF under Grant Nos. DMR-0093217 and CMS-040403.

*Present address: School of Physics and Information Technology, Shaanxi Normal University, Xi'an, Shaanxi 710062, China.

[1] K. Schwab, E. A. Henriksen, J. M. Worlock, and M. L. Roukes, Nature (London) **404**, 974 (2000).
[2] C. S. Yung, D. R. Schmidt, and A. N. Cleland, Appl. Phys. Lett. **81**, 31 (2002).
[3] M. L. Roukes, Physica B **263**, 1 (1999).
[4] I. Bargatin and M. L. Roukes, Phys. Rev. Lett. **91**, 138302 (2003).
[5] D. H. Santamore, A. C. Doherty, and M. C. Cross, Phys. Rev. B **70**, 144301 (2004).
[6] A. N. Cleland and M. R. Geller, Phys. Rev. Lett. **93**, 070501 (2004).
[7] A. D. Armour, M. P. Blencowe, and K. C. Schwab, Phys. Rev. Lett. **88**, 148301 (2002).
[8] R. G. Knobel and A. N. Cleland, Nature (London) **424**, 291

(2003).
[9] A. Cho, Science **299**, 36 (2003).
[10] M. D. LaHaye, O. Buu, B. Camarota, and K. C. Schwab, Science **304**, 74 (2004).
[11] M. P. Blencowe, Phys. Rep. **395**, 159 (2004).
[12] M. P. Blencowe, Science **304**, 56 (2004).
[13] D. R. Schmidt, C. S. Yung, and A. N. Cleland, Appl. Phys. Lett. **83**, 1002 (2003).
[14] D. R. Schmidt, C. S. Yung, and A. N. Cleland, Phys. Rev. B **69**, 140301(R) (2004).
[15] X. Zou and W. Mathis, Phys. Lett. A **324**, 484 (2004).
[16] M. R. Geller and A. N. Cleland, Phys. Rev. A **71**, 032311 (2005).
[17] V. F. Gantmakher, Rep. Prog. Phys. **37**, 317 (1974).
[18] F. C. Wellstood, C. Urbina, and J. Clarke, Phys. Rev. B **49**, 5942 (1994).
[19] M. L. Roukes, M. R. Freeman, R. S. Germain, R. C. Richardson, and M. B. Ketchen, Phys. Rev. Lett. **55**, 422 (1985).
[20] W. A. Little, Can. J. Phys. **37**, 334 (1959).
[21] J. Liu and N. Giordano, Phys. Rev. B **43**, 3928 (1991).
[22] J. F. DiTusa, K. Lin, M. Park, M. S. Isaacson, and J. M. Parpia, Phys. Rev. Lett. **68**, 1156 (1992).
[23] Recall that, in elasticity theory, the mass-density fluctuation $\delta\rho$ is given by $-\rho\nabla\cdot\mathbf{u}$.
[24] P. B. Allen, Phys. Rev. Lett. **59**, 1460 (1987).
[25] H. Ezawa, Ann. Phys. (N.Y.) **67**, 438 (1971).
[26] In the free-electron gas approximation, the Fermi energy of Cu is 7.03 eV, the DOS at ϵ_F is 1.13×10^{34} erg^{-1} cm^{-3}, and v_F is 1.57×10^8 cm s^{-1}.
[27] Cu has the low-temperature elastic constants $c_{11}=1.76\times10^{12}$ dyne cm^{-2}, $c_{12}=1.25\times10^{12}$ dyne cm^{-2}, and $c_{44}=8.18\times10^{11}$ dyne cm^{-2} [see W. C. Overton and J. Gaffney, Phys. Rev. **98**, 969 (1955)], and its mass density is $\rho=8.94$ g cm^{-3}. To approximate a cubic material as an isotropic elastic continuum we define effective elastic constants $C_{11}\equiv c_{11}-2\Delta$ and $C_{44}\equiv c_{44}+\Delta$, where $\Delta\equiv(c_{11}-c_{12}-2c_{44})/5$, and we let $v_l=(C_{11}/\rho)^{1/2}$ and $v_t=(C_{44}/\rho)^{1/2}$. This leads to $v_l=4.97\times10^5$ cm s^{-1}.
[28] D. L. Martin, Phys. Rev. B **8**, 5357 (1973).
[29] M. J. G. Lee, Phys. Rev. B **2**, 250 (1970).
[30] B. Lengeler, W. R. Wampler, R. R. Bourassa, K. Mika, K. Wingerath, and W. Uelhoff, Phys. Rev. B **15**, 5493 (1977).
[31] J. Rammer and A. Schmid, Phys. Rev. B **34**, R1352 (1986).
[32] J. T. Karvonen, L. J. Taskinen, and I. J. Maasilta, Phys. Rev. B **72**, 012302 (2005).
[33] T. Klitsner and R. O. Pohl, Phys. Rev. B **36**, 6551 (1987).